

Decoding in Geometry: Alleviating Embedding-Space Crowding for Complex Reasoning

Yixin Yang¹ Qingxiu Dong¹ Zhifang Sui¹

Abstract

Sampling-based decoding underlies complex reasoning in large language models (LLMs), where decoding strategies critically shape model behavior. Temperature- and truncation-based methods reshape the next-token distribution through global probability reweighting or thresholding to balance the quality-diversity tradeoff. However, they operate solely on token probabilities, ignoring fine-grained relationships among tokens in the embedding space. We uncover a novel phenomenon, *embedding-space crowding*, where the next-token distribution concentrates its probability mass on geometrically close tokens in the embedding space. We quantify crowding at multiple granularities and find a statistical association with reasoning success in mathematical problem solving. Motivated by this finding, we propose CraEG, a plug-in sampling method that mitigates crowding through geometry-guided reweighting. CraEG is training-free, single-pass, and compatible with standard sampling strategies. Experiments on multiple models and benchmarks demonstrate improved generation performance, with gains in robustness and diversity metrics.

1. Introduction

Large language models (LLMs) have recently made substantial progress in complex reasoning (Kaplan et al., 2020; Achiam et al., 2023). In these settings, model outputs are largely determined by autoregressive decoding, where token sampling serves as the fundamental operation. Decoding strategies can therefore have a significant impact on the resulting generations (Shi et al., 2024). Sampling-based decoding has proven particularly effective for LLMs by selecting each next token from the model’s predicted next-

¹State Key Laboratory of Multimedia Information Processing, School of Computer Science, Peking University. Correspondence to: Yixin Yang <yangyx@stu.pku.edu.cn>, Zhifang Sui <szf@pku.edu.cn>.

Preprint. February 2, 2026.

token distribution. It remains the prevailing method for open-ended generation and reasoning (Chowdhery et al., 2023; Guo et al., 2025). Prior work mainly falls into two categories: truncation-based sampling (e.g., top- p (Holtzman et al., 2019), top- k (Fan et al., 2018)) and temperature-based sampling (e.g., Temperature Scaling (Ackley et al., 1985), EDT (Zhang et al., 2024)). By modulating the cut-off threshold or the temperature parameter, these methods globally modify the token probability distribution through truncation, sharpening, or smoothing to better balance the *quality-diversity tradeoff*.

In this work, we study decoding through a geometry-aware view of the next-token distribution, and diagnose its effect on generation behavior. We uncover a novel and under-explored phenomenon, which we term *embedding-space crowding*. This phenomenon occurs when the next-token distribution concentrates its probability mass in a narrow region of the embedding space. We formalize and quantify embedding-space crowding at multiple granularities, and analyze its relationship with reasoning outcomes. Specifically, we use mathematical reasoning as a controlled testbed, where the task is well-defined and correctness is automatically verifiable. Across the AIME benchmark with the Qwen model, our analysis shows that both sequence-level and step-level crowding score are statistically associated with final answer correctness. These findings suggest a statistically significant association between embedding-space crowding and reasoning success, a factor largely unaddressed by prior decoding approaches.

Inspired by this discovery, we propose **Crowding-Aware Sampling via Embedding Geometry** (CraEG), a novel plug-in decoding method that alleviating embedding-space crowding and improves the quality-diversity tradeoff in generation. Specifically, CraEG applies a geometry-guided reweighting scheme to the next-token distribution, downweighting higher-probability, higher-crowding tokens with step-adaptive strength. By reducing redundancy in the embedding space, CraEG promotes sampling beyond narrow, crowded regions, enabling more diverse and robust reasoning trajectories. Moreover, CraEG is training-free, requires no additional supervision or auxiliary models, and introduces no extra forward passes. It is also compatible with

common sampling strategies such as top- p and temperature scaling.

We demonstrate the effectiveness of CraEG across multiple models and evaluation settings. Experiments are conducted with Qwen3-1.7B (Yang et al., 2025), Qwen3-4B, and Hunyuan-1.8B (Tencent, 2025) on three challenging mathematical reasoning benchmarks. We adopt standard sampling configurations, with top- p sampling and temperature scaling as strong baselines. We find that CraEG improves generation performance across diverse settings, with gains on robustness and diversity metrics. For instance, on Qwen3-1.7B (temperature = 1, top- p = 1), CraEG improves avg@32 by 0.52 points and pass@8 by 1.98 percentage points, with gains of 1.17 points in distinct- n and 0.62 points in semantic diversity. Our main contributions are as follows:

- We uncover and formalize *embedding-space crowding*, a decoding phenomenon where next-token probability mass concentrates locally in embedding space.
- We propose quantitative crowding measures and show their statistical association with reasoning success on challenging mathematical reasoning benchmarks.
- We introduce CraEG, a training-free, plug-in decoding method that uses geometry-guided reweighting to alleviate crowding and reduce embedding redundancy.
- We demonstrate the effectiveness of CraEG across multiple models, benchmarks and evaluation settings, improving robustness and diversity metrics under standard sampling baselines.

2. Related Work

Sampling-Based Decoding Methods. Sampling-based decoding dominates open-ended generation and complex reasoning in LLMs (Guo et al., 2025; Shi et al., 2024; Chowdhery et al., 2023). To achieve a better quality-diversity tradeoff, existing methods mainly fall into two categories. Truncation-based methods limit the sampling space to avoid instability from low-probability tokens. Top- p (Holtzman et al., 2019) selects tokens with cumulative probability above p , while top- k (Fan et al., 2018) and ϵ -sampling (Freitag et al., 2023) use fixed counts or probability thresholds. Recent methods further adapt truncation thresholds based on different uncertainty signals, such as entropy (Hewitt et al., 2022; Tan et al., 2025), confidence (Nguyen et al., 2024), or perplexity (Basu et al., 2020). Temperature-based methods modify the overall probability distribution by scaling logits or probabilities with the temperature parameter. Temperature scaling (Ackley et al., 1985) applies a fixed temperature. Other works (Zhang et al., 2024;

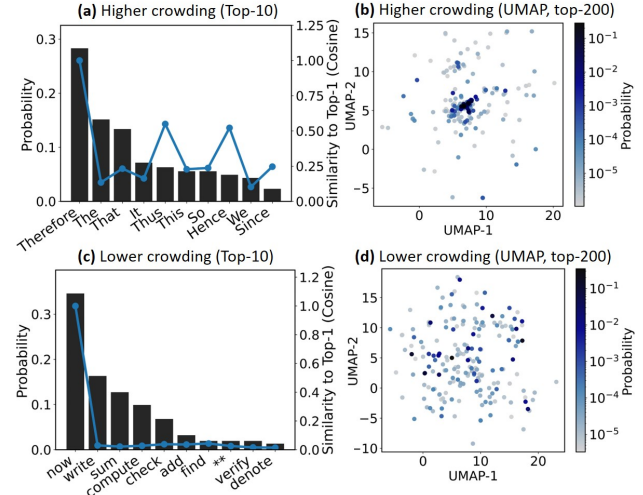


Figure 1. Examples of embedding-space crowding in next-token distributions. We compare two decoding states from the same AIME25 solution trajectory with similar entropy but different crowding levels (higher: Step 447; lower: Step 2003). Left panels show the top-10 probabilities and similarity to the top candidate; right panels show a UMAP projection of the top-200 tokens colored by probability. Higher crowding concentrates probability mass on geometrically similar tokens; lower crowding is more dispersed.

Zhu et al., 2024) dynamically adjusts the temperature at each decoding step based on uncertainty signals. Recent studies (Wang et al., 2025; Troshin et al., 2025) further employ lightweight models to dynamically predict suitable temperature and truncation thresholds during decoding. However, such methods remain restricted to coarse-grained distribution control, ignoring the properties of individual tokens. Other approaches, including guided (Dathathri et al., 2019; Pynadath & Zhang, 2025) and contrastive decoding (Liu et al., 2021; Zhao et al., 2024b), use external signals or auxiliary models to control attributes or enhance generation quality. These methods differ substantially by requiring external or auxiliary preference signals and are complementary to CraEG, as well as to truncation- and temperature-based approaches.

Geometry of Token Representations in LLMs. Token embeddings form the backbone of LLMs, and their geometry has been extensively studied. Some works explore the intrinsic geometry of token embedding spaces, highlighting properties such as dimensionality (Kataiwa et al., 2025), anisotropy (Godey et al., 2024), stratified manifolds (Robinson et al., 2024), and hierarchical structures (Park et al., 2024). Others examine the geometric alignment and transferability of token embeddings across models of different scales, modalities (Wang et al., 2024), and languages (Lee et al., 2025). Additionally, studies (Chen et al., 2025; Robinson et al., 2025a) investigate anomalies in token representa-

tions and their impact on embedding geometry and model performance. Some works (Zhao et al., 2024a; Robinson et al., 2025b) explore how token embedding geometry and topology influence downstream tasks. Prior work has focused primarily on static representations, while we investigate how embedding geometry interacts with probability mass during decoding to shape generation trajectories.

Inference-Time Methods for Reasoning in LLMs.

Many methods improve reasoning quality and diversity by intervening in the generation process. Self-consistency (Wang et al., 2022) and Best-of-N (Shi et al., 2025; Meyerson et al., 2025) generate multiple candidates and select the optimal result based on consistency or coverage. Predictive Sampling (Ma et al., 2024; Xu et al., 2025) and Search-Based Reasoning (Yao et al., 2023; Hamm, 2025) optimize current decisions by simulating future steps. Self-Refine (Madaan et al., 2023) and Guided Decoding (Xie et al., 2023) use self-evaluation to iteratively improve output or guide decoding. Additionally, approaches like tool calls (Yao et al., 2022) and external validators (Ling et al., 2023) adjust or post-process model outputs using external signals. These methods enhance reasoning but differ significantly in complexity, making them complementary to approaches like CraEG, truncation, and temperature scaling. In comparison, our work introduces a crowd-aware decoding strategy, focusing on single-step reweighting without external signals or additional model computations.

3. Embedding-space Crowding in Decoding

In this section, we identify an underexplored phenomenon in LLM decoding, which we term embedding-space crowding. Embedding-space crowding characterizes decoding states in which probability mass is concentrated on tokens that are geometrically close in embedding space, as illustrated in Figure 1. We formally define this notion and introduce quantitative measures of crowding at multiple granularities. Empirically, we find that higher embedding-space crowding is statistically associated with lower reasoning success.

3.1. Defining Embedding-Space Crowding

We define embedding-space crowding on the next-token distribution at each decoding step. It describes how probability mass is arranged in embedding space. Crowding is high when a large share of mass falls on tokens that are close under a given similarity metric, forming a compact region. Crowding differs from widely-used uncertainty metrics in decoding by accounting for geometric relationships among token embeddings. In what follows, we formalize this intuition by measuring how probability mass concentrates around geometrically similar tokens.

Definition 3.1 (Token-Level Crowding Score). Consider a

language model at a given decoding step t with next-token probability distribution $\{p_{t,j}\}_{j \in V}$ and corresponding token embeddings $\{e_j\}_{j \in V}$. The *token-level embedding-space crowding score* of a token i is defined as

$$\text{Crowd}_t^{\text{token}}(i) = \sum_{j \neq i} p_{t,j} |\cos(e_i, e_j)|, \quad (1)$$

where V denotes the vocabulary and $\cos(\cdot, \cdot)$ denotes cosine similarity between embeddings.

Under Definition 3.1, a token-level crowding score reflects the probability-weighted concentration of alternative tokens relative to token i in embedding space. A token has high crowding when other geometrically similar tokens carry non-negligible probability mass. It has low crowding when few plausible alternatives lie nearby. Specifically, we use absolute cosine similarity to measure geometric association strength independent of sign. This treats embeddings pointing in the same or opposite directions as equally associated, since both indicate near-collinearity in embedding space.

Definition 3.2 (Step-Level Crowding Score). Given the token-level crowding scores, we define the *step-level embedding-space crowding score* at decoding step t as

$$\text{Crowd}^{\text{step}}(t) = \sum_i p_{t,i} \cdot \text{Crowd}_t^{\text{token}}(i), \quad (2)$$

Reasoning success is measured at the level of the entire generation sequence. To enable a more direct diagnosis, we further define step-level and sequence-level crowding scores based on the token-level definition. Step-level crowding score is the expected token-level crowding under the next-token distribution at step t (Definition 3.2). It is high when probability mass concentrates on multiple geometrically similar tokens, reflecting competition among close alternatives. It is low when mass either spreads across geometrically diverse tokens or collapses onto a single token, in both cases exhibiting little geometric redundancy. We further extend this to the sequence level by averaging step-level crowding across decoding steps, which yields the average crowding over an entire generation (Definition 3.3).

Definition 3.3 (Sequence-Level Crowding Score). For a generated sequence consisting of T decoding steps, we define the *sequence-level embedding-space crowding score* as

$$\text{Crowd}^{\text{seq}} = \frac{1}{T} \sum_{t=1}^T \text{Crowd}^{\text{step}}(t), \quad (3)$$

In practice, computing crowding scores over the full vocabulary is unnecessary, since low-probability tokens contribute negligibly. We approximate the sums in our crowding scores by restricting computation to a subset $S \subset V$ that contains the top- K tokens under the next-token distribution at each

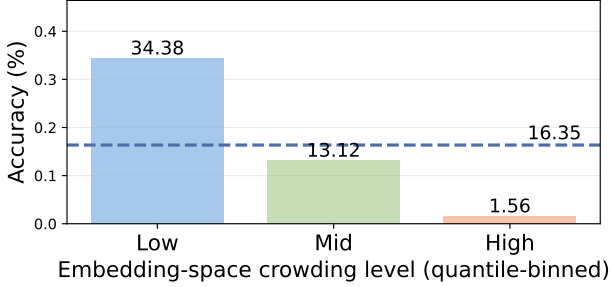


Figure 2. Sequences are binned into low/mid/high groups by quantiles of sequence-level crowding. Bars report accuracy per bin, which decreases monotonically with crowding.

step. This greatly reduces computational cost while retaining most of the probability mass. We use a fixed K throughout our analyses in Section 3.2.

3.2. Empirical Analysis of Embedding-Space Crowding

We study embedding-space crowding on mathematical reasoning using the AIME25 benchmark (Examination, 2025), which contains 30 problems with exact numeric answers. For each problem, we generate 32 samples with temperature 1.0 and top- p 1.0, yielding 960 reasoning traces. We use Qwen3-0.6B (Yang et al., 2025) as a case study because it offers basic complex-reasoning capability while remaining computationally tractable. At each decoding step, we compute token- and step-level crowding from the next-token distribution over the top- K tokens ($K = 100$). Sequence-level crowding is the average step-level crowding over the full generation, as defined in Section 3.1. We evaluate correctness by exact matching of the final numeric answer (Hendrycks et al., 2021). Our analysis at both the sequence and step levels confirms a significant negative association between crowding and reasoning success.

Sequence-level analysis. We analyze the association between sequence-level crowding and reasoning correctness. We bucket sequences into tertiles (low/mid/high) by crowding to form equal-sized groups. Figure 2 shows that accuracy decreases monotonically with crowding, dropping from 34.37% (low) to 13.13% (mid) and 1.56% (high). We further validate this trend by treating crowding continuously. The point-biserial correlation between crowding and correctness is significantly negative ($r = -0.39$, $p = 1.38 \times 10^{-36}$). Overall, these results indicate a significant negative association between embedding-space crowding and reasoning success.

Step-level analysis. To test whether the sequence-level association between crowding and correctness is driven by a small fraction of high-crowding steps, we conduct a comple-

mentary step-level analysis. We pool decoding steps across all samples and group them by the final correctness of their parent sample. As a descriptive comparison, the step-level ECDFs in Appendix 5 show a general rightward shift toward higher crowding for steps from incorrect samples. Elevated crowding is broadly present across steps rather than confined to a few extremes.

Relationship with uncertainty. We use the Shannon entropy (Shannon, 1948) of the next-token distribution as a decoding-time conventional uncertainty measure. While entropy captures overall dispersion, crowding captures how probability mass is organized in embedding space. A logistic regression with standardized sequence-level crowding and average entropy shows that crowding remains a significant negative predictor of correctness (odds ratio = 0.29, $p = 0.001$), whereas entropy is not significant (odds ratio = 0.63, $p = 0.26$). Full regression results and additional visualizations are provided in Appendix B and Appendix C.

4. Method

Motivated by the empirical analyses in Section 3.1, we introduce CraEG, a novel plug-in decoding method that alleviates embedding-space crowding and improves the quality-diversity tradeoff in generation. CraEG applies a geometry-aware reweighting scheme to the next-token distribution, downweighting higher-probability, higher-crowding tokens. Given the negative association between crowding and reasoning success, this encourages more robust decoding on complex reasoning tasks. Furthermore, by promoting sampling beyond narrow, crowded regions, CraEG naturally fosters more diverse reasoning trajectories.

4.1. Method Overview

In autoregressive generation, a language model predicts a next-token distribution over the vocabulary conditioned on the preceding context, and samples a token at each decoding step. Formally, at decoding step t , let V denote the vocabulary and let $P(x_t | x_{1:t-1})$ denote the model’s next-token distribution. Decoding under CraEG proceeds as follows:

Step 1: Selecting an effective correction set. To improve computational efficiency and to avoid unnecessary intervention, we apply corrections only where embedding-space crowding is most pronounced. Specifically, we restrict the correction to non-negligible tokens by defining $S_t = \{i | p_{t,i} \geq \varepsilon\}$ at decoding step t , where ε is a fixed threshold.

Step 2: Computing token- and step-level crowding. Following Definitions 3.1–3.2, we compute crowding within the effective correction set S , which gives us the specific

crowding measures for the current tokens and the step. For each $i \in S$ with probability p_i , token-level crowding is

$$\text{Crowd}_t^{\text{token}}(i) = \sum_{j \in S_t \setminus \{i\}} p_{t,j} |\cos(e_i, e_j)|. \quad (4)$$

We then compute $\text{Crowd}^{\text{step}\dagger}(t)$, an adjusted (nonlinearly weighted) variant of step-level crowding, by aggregating token-level crowding at decoding step t :

$$\text{Crowd}^{\text{step}\dagger}(t) = \sum_{i \in S_t} p_{t,i} (e^{p_{t,i}} - 1) \text{Crowd}_t^{\text{token}}(i). \quad (5)$$

Step 3: Computing correction factors. We compute a step-level correction strength factor λ_t to control the overall distribution adjustment. This factor combines the step-level adjusted crowding from Eq. 5 with the probability mass over S . The hyperparameter $\tau \in [0, 1]$ modulates the global correction strength, where higher values of τ correspond to stronger correction:

$$\lambda_t = \frac{\tau \sum_{i \in S_t} p_i}{\text{Crowd}^{\text{step}\dagger}(t) (1 - \tau \sum_{i \in S} p_i)}. \quad (6)$$

We then combine this with Eq. 4 to obtain a token-wise crowding-aware correction factor α_i for each $i \in S$. This factor is used directly to adjust the next-token distribution, penalizing tokens with both higher probability and higher crowding:

$$\alpha_{t,i} = \frac{1}{1 + \lambda_t (e^{p_{t,i}} - 1) \text{Crowd}_t^{\text{token}}(i)}. \quad (7)$$

Step 4: Crowding-aware correction. For each $i \in S$, we reweight the token by applying α_i , downweighting tokens that have both higher probability and a higher embedding-space crowding score:

$$\tilde{p}_{t,i} = \alpha_{t,i} p_{t,i}. \quad (8)$$

Step 5: Renormalization and reinsertion. We rescale $\{\tilde{p}_{t,i}\}_{i \in S_t}$ to preserve the original mass $\sum_{i \in S_t} p_{t,i}$ and form the final distribution over V :

$$p'_{t,i} = \begin{cases} \tilde{p}_{t,i} \cdot \frac{\sum_{k \in S_t} p_{t,k}}{\sum_{k \in S_t} \tilde{p}_{t,k}}, & i \in S_t, \\ p_{t,i}, & i \in V \setminus S_t. \end{cases} \quad (9)$$

All subsequent sampling is performed from $\{p'_i\}_{i \in V}$.

4.2. Theoretical Intuition and Design Rationale

Building on Section 3, we establish a statistically significant negative correlation between embedding-space crowding

and reasoning success. Embedding-space crowding is a decoding-time phenomenon where probability mass concentrates on geometrically correlated tokens. This overconcentration can bias sampling toward a narrow region of the token space. It can reduce trajectory diversity and restrict how decoding evolves, which may lead to brittle or incorrect generations. Motivated by this intuition, CraEG applies a crowd-aware correction mechanism during sampling to promote more robust and diverse reasoning trajectories. We now detail the design and rationale of its core components: (1) the effective correction set, (2) the token-level crowding-aware correction factor, (3) the step-level correction strength factor, and (4) renormalization.

Effective Correction Set Design. For efficiency and stability, we apply crowding-aware correction only to high-probability tokens in an effective correction set. Crowding is most pronounced on geometrically correlated, high-probability tokens. Correcting the low-probability tail is inefficient due to its limited impact on decoding, introducing unnecessary computation and intervention. We therefore use $S = \{i \mid p_i \geq \varepsilon\}$ with a fixed threshold ε (default $\varepsilon = 10^{-2}$). This choice balances coverage of salient candidates and computational cost. We evaluate alternative thresholds in ablations.

Crowding-aware Correction Factor Design. The correction factor α_i modulates each token according to its probability and embedding-space crowding, suppressing overly concentrated regions while preserving the model’s distributional shape. It acts as a multiplicative down-weighting term. Specifically, tokens with higher probability and stronger embedding redundancy receive larger penalties, whereas lower-probability or less crowded tokens are minimally affected. The exponential term $(e^{p_i} - 1)$ introduces a smooth nonlinear weighting mechanism. This design increases penalization for high-probability tokens under comparable crowding, without overly suppressing lower-probability candidates. Overall, this design enables CraEG to effectively suppress dominant but redundant tokens without relying on additional global heuristics or uncertainty-based metrics.

Correction Strength Factor Design. At decoding step t , the step-level strength factor λ_t controls the overall correction magnitude applied by CraEG to the current distribution. We choose λ_t so that the total probability mass removed from the candidate set S is approximately $\tau \sum_{i \in S} p_i$, which reduces the original mass over S by a fraction τ . This ensures stable and interpretable control and adapts across different distribution shapes and temperature settings. The hyperparameter $\tau \in [0, 1]$ tunes the overall strength. Larger τ applies a stronger correction, while smaller τ better preserves the original distribution. We provide the derivation of λ_t in the detailed Appendix D.

Renormalization. We rescale the penalized probabilities $\{\tilde{p}_{t,i}\}_{i \in S_t}$ to preserve the original total mass of the correction set, $\sum_{i \in S_t} p_{t,i}$. These rescaled values are then merged back into the full vocabulary distribution. Tokens with higher initial probability and crowding are penalized more heavily during correction, resulting in lower probabilities after renormalization. Conversely, tokens less affected by crowding are relatively boosted. Thus, probability mass is systematically shifted away from high-crowding, high-probability regions. Furthermore, by restricting modifications to the effective candidate set S_t , we avoid unnecessary perturbations to the long-tail tokens, which minimizes the introduction of additional noise and randomness.

4.3. Advantages of CraEG for Sampling

CraEG introduces a crowding-aware reweighting mechanism for sampling-based decoding with several advantages. First, CraEG leverages the geometric structure of token embeddings to capture the internal organization of the next-token distribution. In contrast, truncation- and temperature-based methods operate solely on probability values, applying global, coarse-grained adjustments to the overall distribution. Second, CraEG performs localized, geometry-aware reweighting of the next-token distribution, focusing correction on high-probability tokens in crowded embedding regions. By comparison, temperature-based methods promote exploration by uniformly flattening the distribution, often at the cost of increased randomness. Third, CraEG operates on the single-step distribution and requires no extra forward passes, rollouts, or external signals. Finally, as a plug-in probability modifier, CraEG can integrate with standard samplers like temperature and top- p , enabling easy deployment.

4.4. Implementation Details

Integration into Decoding Pipelines. Designed for easy adoption, CraEG acts as a lightweight, post-softmax reweighting step. It can be integrated into standard decoding pipelines without any fine-tuning or architectural changes. As it relies solely on the model’s existing token embeddings and the next-token logits, it is compatible with any open-source LLM. Crowd-aware sampling is also compatible with common sampling methods such as top- k , top- p , and temperature scaling. In practice, CraEG can be inserted between the temperature scaling process and any subsequent filtering step.

Token Embedding Access and Computation. At each decoding step, we use the static embedding vectors for all candidate tokens in the correction set S_t . The token-level crowding score is computed based on pairwise cosine similarities. The scores are computed in two vectorized steps. A pairwise similarity matrix is derived from the candidate

embeddings, followed by a row-wise aggregation to produce the final token-level crowding measure. Since the effective correction set S_t is limited in size (typically $|S_t| \leq 100$ for $\epsilon = 10^{-2}$), its computation, along with the subsequent aggregation, amounts to negligible overhead and is implemented with standard, vectorized tensor operations.

5. Experiments

5.1. Experiments Setup

Models. We adopt Qwen3-1.7B (Yang et al., 2025) as our backbone, as it offers a favorable tradeoff between capability and computational cost and has been used in several recent studies (Ulli & Mondal, 2025; Li et al., 2025). We further evaluate our method on Qwen3-4B (Yang et al., 2025) and Hunyuan-1.8B-Instruct (Tencent, 2025) to assess its robustness and generalizability across different backbone models.

Benchmarks. Mathematical reasoning datasets feature well-defined problems with verifiable answers, making them an ideal testbed for assessing complex reasoning capability. We evaluate CraEG on three representative benchmarks: AIME24 (Examination, 2024), AIME25 (Examination, 2025), and HMMT25 (Tournament, 2025).

Baselines and Hyperparameters. We adopt standard decoding settings as our baseline (top- p nucleus sampling with temperature) and compare CraEG against the same setup without CraEG to control for decoding settings. Experiments were conducted under two common sampling configurations in our main experiments: (1) temperature = 1.0, top- p = 1.0 and (2) temperature = 0.7, top- p = 0.95. All other experiments on different models use the same setup as configuration (1). In the CraEG hyperparameters, setting ϵ to 0.01 and $\tau \in \{0.2, 0.3, 0.4, 0.5\}$ leads to good performance. For more details, please refer to Appendix F.

Evaluation Metrics. For each benchmark, we replicate the evaluation set 32 times and report avg@32, pass@8, Distinct- n , and semantic diversity. Avg@32 is the mean score over 32 repeated runs, indicating result stability. Pass@8 is the fraction of problems solved in at least one of 8 independent trials, following (Chen, 2021). Distinct- n (Jiwei et al., 2016) (with $n = 4$) is the ratio of unique n-grams to total n-grams in the generated set, measuring diversity in the form of language. Semantic diversity is computed from embeddings using all-MiniLM-L12-v2 model (sentence-transformers, 2021). We define $m_{\text{div}} = 1 - \frac{1}{|\mathcal{P}|} \sum_{(i,j) \in \mathcal{P}} \cos(z_i, z_j)$, where \mathcal{P} is the set of all unordered pairs and z_i denotes the embedding of sample i (Tevet & Jonathan, 2021). For efficiency and context-length constraints, semantic diversity uses only the first 512 tokens of each sample’s final output. For presentation in tables, this score is scaled by 100.

Table 1. The results of our main experiments under the two configurations. CraEG enhances both robustness and diversity in reasoning. The metric Dist-n and SemDiv correspond to Distinct-n and Semantic Diversity. Across datasets and both decoding configurations, CraEG generally improves reasoning performance and diversity relative to standard sampling.

AIME24				AIME25				HMMT25							
	Avg@32	Pass@8	Dist-N	SemDiv		Avg@32	Pass@8	Dist-N	SemDiv		Avg@32	Pass@8	Dist-N	SemDiv	
<i>Temp = 1.0, Top-p = 1.0</i>															
Standard Sampling	33.75	55.07	51.00	15.17	35.94	57.33	50.36	16.61	13.85	27.74	51.01	14.78			
+ CraEG (Ours)	34.06	56.59	51.91	15.25	36.46	58.91	52.03	17.70	14.58	30.58	51.93	15.46			
<i>Temp = 0.7, Top-p = 0.95</i>															
Standard Sampling	34.17	57.53	44.70	12.43	35.73	58.69	43.18	14.71	11.88	21.44	41.53	12.02			
+ CraEG (Ours)	34.58	56.16	44.76	12.52	37.29	60.37	44.46	14.50	12.60	24.43	42.28	12.10			

Table 2. The results of experiments on Qwen3-4B model under the configuration (1). CraEG delivers consistent or improved on avg@32 and diversity metrics across benchmarks.

	Avg@32	Pass@8	Dist-N	SemDiv
AIME24				
Standard Sampling	50.42	60.96	51.14	14.99
+ CraEG (Ours)	50.63	60.68	54.60	16.30
AIME25				
Standard Sampling	65.00	81.79	52.37	16.30
+ CraEG (Ours)	65.21	82.47	55.34	17.36
HMMT25				
Standard Sampling	23.75	31.82	51.56	14.78
+ CraEG (Ours)	25.31	33.75	54.17	15.10

5.2. Results

Main Results. For our main experiments, we evaluate Qwen3-1.7B under two decoding configurations, as shown Table 1. Across datasets and settings, CraEG yields consistent gains in Avg@32 and improves overall pass rate and diversity metrics on average. With temperature = 1.0 and top- p = 1.0, CraEG improves Avg@32 by +0.52 points and Pass@8 by +1.98 points on average, while also increasing Dist-N (+1.17) and semantic diversity (+0.62). Under a more conservative setting with temperature = 0.7, top- p = 0.95, CraEG continues to improve Avg@32 (+0.90) and Pass@8 (+1.10) on average and modestly increases Dist-N (+0.70), while semantic diversity remains essentially unchanged (-0.01 on average). These results show that CraEG generally improves reasoning performance and diversity relative to standard sampling across datasets and both decoding configurations.

Beyond the averaged gains, we observe that the benefits of CraEG depend on the decoding configurations. Diversity improvements are more pronounced at $T=1.0$, $top-p=1.0$, while remaining modest under $T=0.7$, $top-p=0.95$ with semantic diversity largely unchanged. This indicates that the diversity gains from CraEG are consistent across decoding configurations. They are larger when sampling permits

broader exploration, and remain measurable under tighter constraints. Notably, Avg@32 improves across all datasets in both configurations, suggesting a more reliable overall generation quality even when individual metrics may occasionally fluctuate. Furthermore, the largest Pass@8 gains are observed on the more challenging HMMT25 benchmark (up to +2.99), indicating that CraEG has the potential to be especially helpful on harder benchmarks.

Table 3. The results of experiments on Hunyuan-1.8B-Instruct model under the configuration (1) on AIME24. CraEG delivers clear accuracy improvements, with small declines in diversity metrics

	Avg@32	Pass@8	Dist-N	SemDiv
Standard Sampling	22.18	35.01	81.54	19.27
+ CraEG (Ours)	23.54	39.94	79.41	18.81

Experiments on Other Models. To examine transferability, we additionally evaluate CraEG on a larger Qwen3-4B model and Hunyuan-1.8B-Instruct as a non-Qwen model. As shown Table 2, on Qwen3-4B, CraEG improves Avg@32 across all three benchmarks and increases diversity metrics, both Dist-N and SemDiv, consistently, while Pass@8 improves on AIME25 and HMMT25 with a minor decrease on AIME24 (-0.28). As shown Table 3, on Hunyuan-1.8B-Instruct with AIME24 benchmark, CraEG improves accuracy, increasing Avg@32 (+1.36) and Pass@8 (+4.93), though Dist-N and SemDiv slightly decrease. Importantly, the fraction of near-exact semantic matches used in SemDiv computation (similarity > 0.999) drops from 1.04% to 0.39%, indicating reduced near-duplicate outputs despite the small change in aggregate diversity scores. Overall, these results suggest that CraEG generalizes beyond the base model, while the diversity-accuracy tradeoff can be model-dependent.

5.3. Ablation Study

To further validate the design of CraEG, we conduct an ablation study using the Qwen3-1.7B model and the AIME25

dataset as representative cases. Our analysis focuses on two key components: the nonlinear weighting mechanism and the step-level correction strength factor.

Table 4. Ablation on nonlinear and linear weighting in CraEG. Both improve over standard sampling, supporting the effectiveness of crowding-aware correction, with complementary accuracy-diversity profiles.

	Avg@32	Pass@8	Dist-N	SemDiv
Standard Sampling	35.94	57.33	50.36	16.61
+ CraEG (Nonlinear)	36.46	58.91	52.03	17.70
+ CraEG (Linear)	39.37	63.47	50.97	17.31

Nonlinear Weighting Mechanism. An exponential term, $(e^{p_{t,i}} - 1)$, is used to construct a smooth penalty function that slightly amplifies the correction for high-probability tokens. As shown in Table 4, replacing $(e^{p_{t,i}} - 1)$ with a linear term p_i still improves over standard sampling. This indicates that the main benefit comes from the crowding-aware correction itself, rather than a specific weighting choice. The two weightings yield different accuracy–diversity profiles. The linear form achieves higher Avg@32 (39.3) and Pass@8 (63.47). The exponential form yields higher diversity, both Dist-N (52.03) and SemDiv (17.70). These results suggest that the nonlinear and linear weighting modulates how strongly probability mass is shifted away from high-probability tokens. Nonlinear reweighting promotes exploration and diversity, but may increase decoding stochasticity. We leave a systematic characterization of this tradeoff, and adaptive weighting schemes, to future work.

Correction Strength Factor. The step-level strength factor λ_t adapts the correction magnitude to each step’s probability distribution for stability. Fixing $\lambda_t = 10$ degrades accuracy. The detailed results and derivation of λ_t are provided in the Appendix E and D.

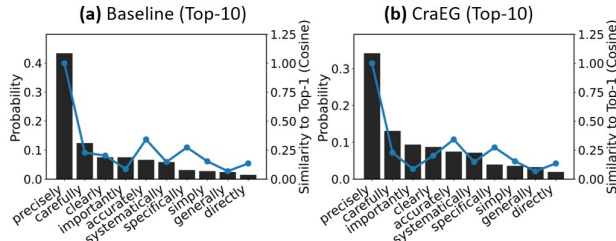


Figure 3. Step-level example of probability reallocation. Top-10 next-token probabilities and cosine similarity to the top-1 candidate (baseline vs. CraEG).

5.4. Case Analysis

Step-level redistribution. To provide intuitive insights into how CraEG reshapes decoding locally, we visualize the

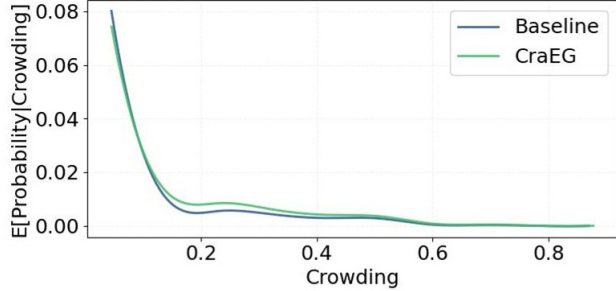


Figure 4. Trajectory-level token crowding analysis (top-30 per step). We report $\mathbb{E}[p | \text{crowding}]$ and the mean crowding aggregated over decoding steps. CraEG reduces the mean from 0.1934 to 0.1864.

top-10 next-token distribution at a representative decoding step (Figure 3). Compared to standard sampling, CraEG assigns slightly different probabilities across the same top-10 candidates, shifting mass from the most dominant option to several close alternatives. **Insight:** the correction refines the model’s preference among the same top-10 candidates, giving more room to plausible alternatives.

Trajectory-level crowding statistics. To provide complementary insights at the sequence level, Figure 4 aggregates token-level crowding over the top-30 candidates along the full decoding trajectory and reports $\mathbb{E}[p | \text{crowding}]$. Compared to the baseline, CraEG assigns slightly higher expected probability in the low-to-moderate crowding regime, while the extreme regions remain similar. Over the entire trajectory, the mean top-30 token-level crowding decreases from 0.1934 (baseline) to 0.1864 (CraEG). **Insight:** CraEG shifts probability mass toward candidates with lower crowding in a gradual, trajectory-wide manner.

6. Conclusion

We take a geometry-based view of LLM decoding and show that embedding-space crowding influences how probability mass concentrates among localized region. Leveraging this perspective, we quantify crowding as a diagnostic signal to analyze how decoding-time crowding is associated with success on complex reasoning. We then propose CraEG, a lightweight crowding-aware sampling method that smoothly reweights next-token probabilities to improves the quality-diversity tradeoff. CraEG improves accuracy and generally strengthens diversity, with case studies revealing consistent trajectory-level shifts toward lower-crowding candidates. These results suggest that incorporating representation geometry into sampling can improve inference robustness and diversity, and motivate future geometry-aware decoding methods.

Impact Statement

This paper presents work whose goal is to advance the field of machine learning by improving decoding for language models. The societal implications are similar to those of other methods that increase the quality and diversity of generated text: they can benefit downstream applications but may also amplify misuse if deployed without appropriate safeguards. We do not foresee impacts beyond these well-established considerations.

References

Achiam, J., Adler, S., Agarwal, S., Ahmad, L., Akkaya, I., Aleman, F. L., Almeida, D., Altenschmidt, J., Altman, S., Anadkat, S., et al. Gpt-4 technical report. *arXiv preprint arXiv:2303.08774*, 2023.

Ackley, D. H., Hinton, G. E., and Sejnowski, T. J. A learning algorithm for boltzmann machines. *Cognitive science*, 9(1):147–169, 1985.

Basu, S., Ramachandran, G. S., Keskar, N. S., and Varshney, L. R. Mirostat: A neural text decoding algorithm that directly controls perplexity. *arXiv preprint arXiv:2007.14966*, 2020.

Chen, K., Wang, D., Liu, Y., Zhang, H., and Wang, W. Sticking to the mean: Detecting sticky tokens in text embedding models. In *Proceedings of the 63rd Annual Meeting of the Association for Computational Linguistics (Volume 1: Long Papers)*, pp. 28660–28681, 2025.

Chen, M. Evaluating large language models trained on code. *arXiv preprint arXiv:2107.03374*, 2021.

Chowdhery, A., Narang, S., Devlin, J., Bosma, M., Mishra, G., Roberts, A., Barham, P., Chung, H. W., Sutton, C., Gehrmann, S., et al. Palm: Scaling language modeling with pathways. *Journal of Machine Learning Research*, 24(240):1–113, 2023.

Dathathri, S., Madotto, A., Lan, J., Hung, J., Frank, E., Molino, P., Yosinski, J., and Liu, R. Plug and play language models: A simple approach to controlled text generation. *arXiv preprint arXiv:1912.02164*, 2019.

Examination, A. I. M. Aime 2024 (i & ii). https://huggingface.co/datasets/HuggingFaceH4/aime_2024, 2024. URL https://huggingface.co/datasets/HuggingFaceH4/aime_2024.

Examination, A. I. M. AIME 2025 (i & ii): A dataset for mathematical reasoning. <https://huggingface.co/datasets/opencompass/AIME2025>, 2025. URL <https://huggingface.co/datasets/opencompass/AIME2025>.

Fan, A., Lewis, M., and Dauphin, Y. Hierarchical neural story generation. *arXiv preprint arXiv:1805.04833*, 2018.

Freitag, M., Ghorbani, B., and Fernandes, P. Epsilon sampling rocks: Investigating sampling strategies for minimum bayes risk decoding for machine translation. *arXiv preprint arXiv:2305.09860*, 2023.

Godey, N., Clergerie, É., and Sagot, B. Anisotropy is inherent to self-attention in transformers. In *Proceedings of the 18th Conference of the European Chapter of the Association for Computational Linguistics (Volume 1: Long Papers)*, pp. 35–48, 2024.

Guo, D., Yang, D., Zhang, H., Song, J., Zhang, R., Xu, R., Zhu, Q., Ma, S., Wang, P., Bi, X., et al. Deepseek-r1: Incentivizing reasoning capability in llms via reinforcement learning. *arXiv preprint arXiv:2501.12948*, 2025.

Hamm, L. Novelty-based tree-of-thought search for llm reasoning and planning neuigkeit-basierte tree-of-thought-suche für llm-planung und-problemlösung. 2025.

Hendrycks, D., Burns, C., Kadavath, S., Arora, A., Basart, S., Tang, E., Song, D., and Steinhardt, J. Measuring mathematical problem solving with the math dataset. *arXiv preprint arXiv:2103.03874*, 2021.

Hewitt, J., Manning, C. D., and Liang, P. Truncation sampling as language model desmothing. *arXiv preprint arXiv:2210.15191*, 2022.

Holtzman, A., Buys, J., Du, L., Forbes, M., and Choi, Y. The curious case of neural text degeneration. *arXiv preprint arXiv:1904.09751*, 2019.

Jiwei, L., Michel, G., Chris, B., Jianfeng, G., and Bill, D. A diversity promoting objective function for neural conversation models. *Proceedings of NAACL*, 2016, 2016.

Kaplan, J., McCandlish, S., Henighan, T., Brown, T. B., Chess, B., Child, R., Gray, S., Radford, A., Wu, J., and Amodei, D. Scaling laws for neural language models. *arXiv preprint arXiv:2001.08361*, 2020.

Kataiwa, T., Hakaze, C., and Ohki, T. Measuring intrinsic dimension of token embeddings. *arXiv preprint arXiv:2503.02142*, 2025.

Langley, P. Crafting papers on machine learning. In Langley, P. (ed.), *Proceedings of the 17th International Conference on Machine Learning (ICML 2000)*, pp. 1207–1216, Stanford, CA, 2000. Morgan Kaufmann.

Lee, A., Weber, M., Viégas, F., and Wattenberg, M. Shared global and local geometry of language model embeddings. *arXiv preprint arXiv:2503.21073*, 2025.

Li, S., Zhou, Z., Lam, W., Yang, C., and Lu, C. Repo: Replay-enhanced policy optimization. *arXiv preprint arXiv:2506.09340*, 2025.

Ling, Z., Fang, Y., Li, X., Huang, Z., Lee, M., Memisevic, R., and Su, H. Deductive verification of chain-of-thought reasoning. *Advances in Neural Information Processing Systems*, 36:36407–36433, 2023.

Liu, A., Sap, M., Lu, X., Swayamdipta, S., Bhagavatula, C., Smith, N. A., and Choi, Y. Dexperts: Decoding-time controlled text generation with experts and anti-experts. *arXiv preprint arXiv:2105.03023*, 2021.

Ma, C., Zhao, H., Zhang, J., He, J., and Kong, L. Non-myopic generation of language models for reasoning and planning. *arXiv preprint arXiv:2410.17195*, 2024.

Madaan, A., Tandon, N., Gupta, P., Hallinan, S., Gao, L., Wiegreffe, S., Alon, U., Dziri, N., Prabhumoye, S., Yang, Y., et al. Self-refine: Iterative refinement with self-feedback. *Advances in Neural Information Processing Systems*, 36:46534–46594, 2023.

Meyerson, E., Paolo, G., Dailey, R., Shahrzad, H., Francon, O., Hayes, C. F., Qiu, X., Hodjat, B., and Miikkulainen, R. Solving a million-step llm task with zero errors. *arXiv preprint arXiv:2511.09030*, 2025.

Nguyen, M. N., Baker, A., Neo, C., Roush, A., Kirsch, A., and Shwartz-Ziv, R. Turning up the heat: Min-p sampling for creative and coherent llm outputs. *arXiv preprint arXiv:2407.01082*, 2024.

Park, K., Choe, Y. J., Jiang, Y., and Veitch, V. The geometry of categorical and hierarchical concepts in large language models. *arXiv preprint arXiv:2406.01506*, 2024.

Pynadath, P. and Zhang, R. Controlled llm decoding via discrete auto-regressive biasing. *arXiv preprint arXiv:2502.03685*, 2025.

Robinson, M., Dey, S., and Sweet, S. The structure of the token space for large language models. *arXiv preprint arXiv:2410.08993*, 2024.

Robinson, M., Dey, S., and Chiang, T. Token embeddings violate the manifold hypothesis. *arXiv preprint arXiv:2504.01002*, 2025a.

Robinson, M., Dey, S., and Kushner, T. Probing the topology of the space of tokens with structured prompts. *Mathematics*, 13(20):3320, 2025b.

sentence-transformers. all-minilm-l12-v2. <https://huggingface.co/sentence-transformers/all-MiniLM-L12-v2>, 2021. Hugging Face model card, accessed 2026-01-21.

Shannon, C. E. A mathematical theory of communication. *The Bell system technical journal*, 27(3):379–423, 1948.

Shi, C., Yang, H., Cai, D., Zhang, Z., Wang, Y., Yang, Y., and Lam, W. A thorough examination of decoding methods in the era of llms. *arXiv preprint arXiv:2402.06925*, 2024.

Shi, W., Cui, Y., Wu, Y., Fang, J., Zhang, S., Li, M., Han, S., Zhu, J., Xu, J., and Zhou, X. Semantic-guided diverse decoding for large language model. *arXiv preprint arXiv:2506.23601*, 2025.

Tan, R., Wu, S., and Howard, P. p-less sampling: A robust hyperparameter-free approach for llm decoding. *arXiv preprint arXiv:2509.23234*, 2025.

Tencent. Hunyuan-1.8b-instruct. <https://huggingface.co/tencent/Hunyuan-1.8B-Instruct>, 2025. Hugging Face model card, accessed 2026-01-21.

Tevet, G. and Jonathan, B. Evaluating the evaluation of diversity in natural language generation. In *Proceedings of the 16th Conference of the European Chapter of the Association for Computational Linguistics: Main Volume*, pp. 326–346, 2021.

Tournament, H.-M. M. Hmmt february 2025 problems. https://huggingface.co/datasets/FlagEval/HMMT_2025, 2025. URL https://huggingface.co/datasets/FlagEval/HMMT_2025.

Troshin, S., Mohammed, W., Meng, Y., Monz, C., Fokkens, A., and Niculae, V. Control the temperature: Selective sampling for diverse and high-quality llm outputs. *arXiv preprint arXiv:2510.01218*, 2025.

Ulli, V. B. and Mondal, A. Medqwen-pe: Medical qwen for parameter-efficient multilingual patient-centric summarization, question answering and information extraction. In *NLP-AI4Health*, pp. 86–92, 2025.

Wang, D., Zuo, Y., Li, F., and Wu, J. Llms as zero-shot graph learners: Alignment of gnn representations with llm token embeddings. *Advances in Neural Information Processing Systems*, 37:5950–5973, 2024.

Wang, X., Wei, J., Schuurmans, D., Le, Q., Chi, E., Narang, S., Chowdhery, A., and Zhou, D. Self-consistency improves chain of thought reasoning in language models. *arXiv preprint arXiv:2203.11171*, 2022.

Wang, Z., Ma, D., Huang, X., Cai, D., Lan, T., Xu, J., Mi, H., Tang, X., and Wang, Y. The end of manual decoding: Towards truly end-to-end language models. *arXiv preprint arXiv:2510.26697*, 2025.

Xie, Y., Kawaguchi, K., Zhao, Y., Zhao, J. X., Kan, M.-Y., He, J., and Xie, M. Self-evaluation guided beam search for reasoning. *Advances in Neural Information Processing Systems*, 36:41618–41650, 2023.

Xu, F., Yan, H., Ma, C., Zhao, H., Liu, J., Lin, Q., and Wu, Z. ϕ -decoding: Adaptive foresight sampling for balanced inference-time exploration and exploitation. *arXiv preprint arXiv:2503.13288*, 2025.

Yang, A., Li, A., Yang, B., Zhang, B., Hui, B., Zheng, B., Yu, B., Gao, C., Huang, C., Lv, C., et al. Qwen3 technical report. *arXiv preprint arXiv:2505.09388*, 2025.

Yao, S., Zhao, J., Yu, D., Du, N., Shafran, I., Narasimhan, K. R., and Cao, Y. React: Synergizing reasoning and acting in language models. In *The eleventh international conference on learning representations*, 2022.

Yao, S., Yu, D., Zhao, J., Shafran, I., Griffiths, T., Cao, Y., and Narasimhan, K. Tree of thoughts: Deliberate problem solving with large language models. *Advances in neural information processing systems*, 36:11809–11822, 2023.

Zhang, S., Bao, Y., and Huang, S. Edt: Improving large language models’ generation by entropy-based dynamic temperature sampling. *arXiv preprint arXiv:2403.14541*, 2024.

Zhao, Y., Behnia, T., Vakilian, V., and Thrampoulidis, C. Implicit geometry of next-token prediction: From language sparsity patterns to model representations. *arXiv preprint arXiv:2408.15417*, 2024a.

Zhao, Z., Monti, E., Lehmann, J., and Assem, H. Enhancing contextual understanding in large language models through contrastive decoding. *arXiv preprint arXiv:2405.02750*, 2024b.

Zhu, Y., Li, J., Li, G., Zhao, Y., Jin, Z., and Mei, H. Hot or cold? adaptive temperature sampling for code generation with large language models. In *Proceedings of the AAAI Conference on Artificial Intelligence*, volume 38, pp. 437–445, 2024.

A. Step-level ECDF analysis

We provide additional step-level evidence complementing the sequence-level results in Section 3.2. We pool all decoding steps from the generated samples and group them by the final correctness of the parent sample. Figure 5 plots the empirical cumulative distribution functions (ECDFs) of step-level crowding for steps from correct and incorrect samples. The incorrect ECDF is generally right-shifted toward higher crowding across most quantiles. Since steps within a sample are not independent, we report this as a descriptive comparison. The observed shift is consistent with elevated crowding being broadly present across steps rather than confined to a small number of extreme steps.

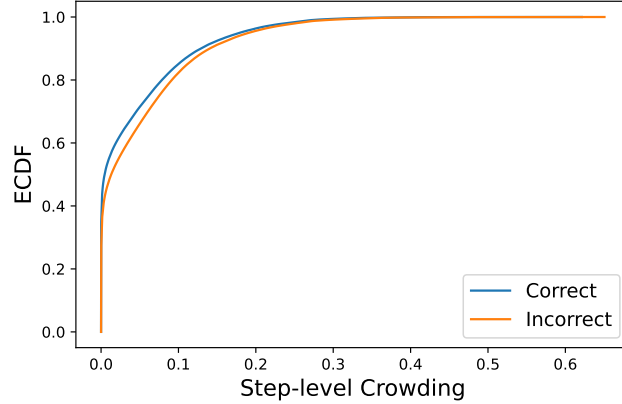


Figure 5. ECDFs of step-level embedding-space crowding. Empirical cumulative distribution functions of step-level crowding for decoding steps from correct and incorrect samples. Steps from incorrect samples are generally right-shifted toward higher crowding, consistent with elevated crowding being broadly present across steps rather than confined to a few extremes.

B. Additional Regression Analysis

We report additional logistic regression results analyzing the relationship between embedding-space crowding, entropy, and reasoning correctness. The model predicts sequence-level correctness from standardized sequence-level crowding and next-token entropy. Coefficients are estimated using maximum likelihood, and odds ratios (OR) are reported for interpretability. Table 5 shows that crowding remains a significant negative predictor of correctness when controlling for entropy, whereas entropy does not exhibit a statistically significant effect.

Table 5. Logistic regression predicting reasoning correctness. Both predictors are standardized. We report odds ratios (OR) and coefficient estimates.

Predictor	OR	Coef	Std. Err.	p-value
Crowding (z)	0.29	-1.25	0.39	0.001
Entropy (z)	0.63	-0.47	0.41	0.26
Intercept	-	-2.39	0.16	< 0.001

C. Visualizing Crowding and Entropy

Figure 6 visualizes the relationship between step-level embedding-space crowding and next-token entropy across all decoding steps. While the two quantities are correlated, their relationship is highly non-linear and exhibits substantial dispersion. In particular, similar entropy values can correspond to a wide range of crowding values, and vice versa. This supports the view that crowding captures geometric structure in the next-token distribution that is not fully characterized by entropy alone.

D. Derivation of the Correction Strength Factor λ_t

To control the overall correction strength at each decoding step, we introduce a hyperparameter $\tau \in [0, 1]$ that modulates how much total probability mass to suppress from the effective correction set. Specifically, we define the target reduction in

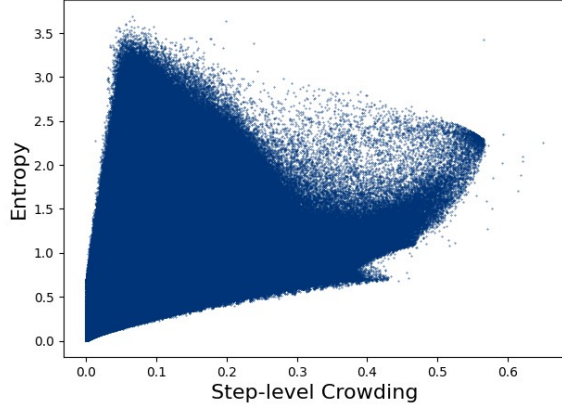


Figure 6. Scatter plot of step-level embedding-space crowding versus next-token entropy. Each point corresponds to a decoding step. The non-linear and dispersed relationship highlights that crowding and entropy capture distinct properties of the next-token distribution.

mass as

$$\delta_t = \tau \cdot \sum_{i \in S_t} p_{t,i}, \quad (10)$$

where $p_{t,i}$ denotes the original softmax probability of token i . This reflects our design goal: downweighting the S_t region by a fraction τ of its total original mass, adapting the strength of correction to the shape of the distribution at each step.

Given each token’s crowding score, we define crowding-aware correction factor for each token (Eq. 5), with an intermediate value $C_{t,i}$:

$$C_{t,i} = (e^{p_{t,i}} - 1) \cdot \text{Crowd}_t^{\text{token}}(i), \quad (11)$$

$$\alpha_{t,i} = \frac{1}{1 + \lambda_t C_{t,i}}. \quad (12)$$

Then, the total reduction can be defined as

$$\Delta_t = \sum_{i \in S_t} p_{t,i} \cdot (1 - \alpha_{t,i}). \quad (13)$$

The scaling factor λ_t is then determined by solving the following implicit equation, which ensures that the actual reduction Δ_t matches the target reduction δ_t :

$$\sum_{i \in S_t} p_{t,i} \cdot \frac{\lambda_t C_{t,i}}{1 + \lambda_t C_{t,i}} = \delta_t. \quad (14)$$

Direct numerical root-finding for Eq. 14 is possible but would undermine the efficiency goal of a plug-in decoder. We therefore derive a practical approximation that admits a closed-form solution. We apply a mean-based approximation by replacing each $C_{t,i}$ in the sum with the weighted average $\mu_t = \sum_{i \in S_t} p_{t,i} C_{t,i}$ (or $\mathbb{E}[C_{t,i}]$), leading to:

$$\sum_{i \in S_t} p_{t,i} \cdot \frac{\lambda_t C_{t,i}}{1 + \lambda_t C_{t,i}} \approx \frac{\lambda_t \mu_t}{1 + \lambda_t \mu_t}. \quad (15)$$

Substituting the approximation into the condition $\Delta_t = \delta_t$ and solving for λ_t provides a closed-form update:

$$\frac{\lambda_t \mu_t}{1 + \lambda_t \mu_t} = \delta_t \implies \lambda_t = \frac{\delta_t}{\mu_t (1 - \delta_t)}. \quad (16)$$

Recalling that $\delta_t = \tau \cdot \sum_{i \in S_t} p_{t,i}$ and $\mu_t = \sum_{i \in S_t} p_{t,i} C_{t,i}$, and substituting them into $\lambda_t = \frac{\delta_t}{\mu_t(1-\delta_t)}$, we arrive at the practical, closed-form solution for the step-level correction strength:

$$\lambda_t = \frac{\tau \cdot \sum_{i \in S_t} p_i}{(\sum_{i \in S_t} p_{t,i} \cdot C_{t,i}) \cdot (1 - \tau \sum_{i \in S} p_i)} = \frac{\tau \cdot \sum_{i \in S_t} p_i}{\text{Crowd}^{\text{step}\dagger}(t) \cdot (1 - \tau \sum_{i \in S} p_i)}. \quad (17)$$

Interpretation. This formulation provides λ_t and τ with a clear, local probabilistic interpretation. Together, they determine the expected fraction of probability mass to be removed from the correction set S_t . Consequently, our method ensures a specified correction strength with τ while dynamically adapting the step-wise strength λ_t to the distribution structure. This dynamic adaptation guarantees that the degree of intervention is scaled appropriately to the prevailing crowding and geometric redundancy.

E. Ablation for Correction Strength Factor

We conducted an ablation study on a subset of AIME25 with 17 samples (Table 6). We observed that when $\lambda_t = 10$, the diversity metric improves while the accuracy performance drops significantly. This aligns with our design rationale: without a Correction Strength Factor that dynamically adjusts according to the distribution and crowding, certain decoding steps may be over- or under-adjusted. Even though it brings benefits in diversity, it does so at the cost of accuracy.

Table 6. Ablation study on the Correction Strength Factor (λ_t). Results on a subset of AIME25 (17 samples) show that a fixed $\lambda_t = 10$ improves diversity but severely harms accuracy, highlighting the need for dynamic adjustment.

	Avg@32	Pass@8	Dist-N	SemDiv
CraEG	46.32	65.31	48.85	16.88
CraEG (Fixed λ_t)	43.38	61.07	49.73	17.40

F. Hyperparameter Details

We provide a detailed specification of the hyperparameter τ used across different models, configuration settings, and benchmarks, as shown in Table 7.

Table 7. Hyperparameter τ used across different models, configuration settings, and benchmark.

Model	Temperature/Top-p	Dataset	Hyper
Qwen3-1.7B	temp=1.0, top-p=1.0	AIME24	0.3
		AIME25	0.3
		HMMT25	0.3
	temp=0.7, top-p=0.95	AIME24	0.3
		AIME25	0.2
		HMMT25	0.2
Qwen3-4B	temp=1.0, top-p=1.0	AIME24	0.5
		AIME25	0.5
		HMMT25	0.4
Hunyuan-1.8B-Instruct	temp=1.0, top-p=1.0	AIME24	0.2